Korean J. Chem. Eng., 37(2), 295-306 (2020)
DOI: 10.1007/s11814-019-0350-7

pISSN: 0256-1115
eISSN: 1975-7220

Influence of functionalized SiO_2 nanoparticles on the morphology and CO_2/CH_4 separation efficiency of Pebax-based mixed-matrix membranes

Maryam Ariazadeh*, Zahra Farashi, Navid Azizi***,†, and Mohammad Khajouei*****

*Mineral Biochemistry Laboratory, Department of Chemistry, Iran University of Science and Technology (IUST), Narmak, Tehran, Iran
**Faculty of Mechanical Engineering, Semnan University, Semnan, Iran
***Department of Chemical Engineering, Shiraz Branch, Islamic Azad University, Shiraz, Iran
****Nanotechnology Research Institute, School of Chemical Engineering, Babol (Noshirvani) University of Technology, Babol, Iran
(*Received 9 May 2019 • accepted 5 August 2019*)

Abstract−Silica (SiO_2) nanoparticles were first functionalized using (3-aminopropyl) triethoxysilane (APTES) and then utilized as filler for the preparation of poly (ether-block-amide) (Pebax®-1074) based mixed-matrix membranes (MMMs). To characterize the modified nanoparticles and the prepared membranes, Fourier transform infrared (FT-IR) spectroscopy, field emission scanning electron microscopy (FESEM), X-ray diffraction (XRD), and thermal gravimetric analysis (TGA) were conducted. The influences of the pure and amine-modified nanoparticles content, and feed temperature and pressure on CO_2 and CH_4 permeability and ideal CO_2/CH_4 selectivity values of the membranes were studied. The permeation experiments exhibited that the incorporation of 12.5 wt% of amine-functionalized SiO_2 nanoparticles into the Pebax matrix raises the CO_2 permeability and ideal CO_2/CH_4 selectivity about 100 and 32%, respectively.

Keywords: Pebax, (3-Aminopropyl) triethoxysilane, SiO_2, CO_2/CH_4 Separation

INTRODUCTION

The use of membrane technology in separation processes has been highly considered due to the high proficiency, simplicity of scale-up and mixing with different processing approaches, low energy necessity, low cost of operation, and moderate operating conditions requirements [1]. Moreover, polymer-based membranes have been preferred to other types of membranes because of their remarkable characteristics like the low production costs and considerable processability. However, as can be seen in Robeson diagrams, a trade-off exists between the features of permeability and selectivity of the polymer-based membranes [1]. Besides, although inorganic materials as base materials for the membrane fabrication show high performance in selectivity and permeability, they are often lowly thermal resistant and problematic to scale-up for use in membrane separation processes. Mixed-matrix membranes (MMMs) are often fabricated by dispersion of minerals into a polymeric matrix to utilize the benefits of each different raw material, to attain highly efficient membranes having simultaneously high permeability and selectivity [2-4].

Among numerous polymeric resources, polyethylene oxide (PEO) is approved to be an operative polymer to separate CO_2 from natural gas streams because of the high affinity of this gas to ethylene oxide groups of the PEO; however, its great tendency for being crystallized leads to the loss of its CO_2 permeability [1]. So, to employ the maximum PEO advantages, block copolymers with the base of PEO have been synthesized, amongst poly (ether-b-amide), a commercially recognized as Pebax®, which has been widely combined with suitable fillers. Pebax® contains two parts: 1) polyether (PE), which causes a good CO_2 permeability, originating from its excellent chain flexibility, as well as good affinity to the polar molecules, and 2) polyamide (PA), which can donate an excellent mechanical steadiness to the polymer due to the glassy nature of the PA [5]. In this study, Pebax®-1074 comprising 55 wt% of PE and 45 wt% of PA was chosen as the base material for the membrane synthesis.

Up to now, several categories of inorganic fillers, such as nonporous particles including SiO_2, TiO_2, Al_2O_3, and ZnO, and porous ones such as metal-organic frameworks (MOFs), zeolites, and multi-walled carbon nanotubes (MWCNTs), have been selected to prepare MMMs [6-9]. Generally, the incorporation of nanoparticles at an optimum loading into a polymer matrix of a MMM would enhance CO_2 gas permeability, while it has different effects on the selectivity. Sometimes it keeps the selectivity nearly constant or in specific cases, reduces the MMM diffusivity selectivity owing to the blockage of the gas molecules penetration paths, resulting from rigidifying the polymer chains [10]. For example, Hwang et al., fabricated MMMs using poly (vinyl chloride)-g-poly (oxyethylene methacrylate) and hollow ZIF-8 and examined for CO_2/CH_4 gas separation. The results indicated that the incorporation of the nanofillers into the polymer matrix enhanced the CO_2 gas permeation but decreased the selectivity slightly [11]. Some other researches have shown that the selectivity rises with enhancing the nanoparticles in a polymer matrix. As an example, Ghadimi et al. prepared MMMs via incorporating SiO_2 into Pebax-1657 matrix. Their

†To whom correspondence should be addressed.
E-mail: n_azizi@iust.ac.ir

results showed that with increasing the nanoparticles in the polymer matrix, the CO_2 permeability, as well as CO_2/CH_4, CO_2/N_2, and CO_2/H_2 selectivities increased [6]. Therefore, in addition to the polymer type, choosing appropriate nanoparticles as the filler is another crucial factor in the synthesis of the practical MMM for the gas separation. SiO_2 nanoparticles regard to the great thermal and mechanical stabilities, appropriate specific surface area, availability, low cost and the facility of chemical modification can be considered as favorable fillers for gas separation membranes [12]. To date, several researchers have investigated the influence of SiO_2 loading on gas permeation characteristics of various polymeric matrices. Most of the results indicate the enhanced gas transport features of the synthesized membranes due to the chain packing disruption of the polymer, thereby the increment of free volume in the polymer phase, as well as the creation of voids at the polymer-particle interface [6,13-16].

Chemical functionalization of nanoparticles with different chemical groups such as amines can be regarded as a useful approach to improving the adsorption efficiency of nanoparticles, as well as the interfacial adaptability of organic and inorganic phases, leading to their better dispersion into the polymer matrix [17]. So far, various aminosilane agents have been utilized to amend different nanoparticles for the fabrication of MMMs apt for CO_2 removal, although a few studies have investigated amine modification of the nanoparticles, being incorporated into different Pebax matrices. Isanejad et al., surface-modified fumed SiO_2 nanoparticles via APTES and employed as the inorganic filler for the fabrication of Pebax-1657-based MMMs for separation of CO_2/CH_4. The gas permeation investigations showed that embedding 15 wt% of the amine-modified silica nanoparticles into the Pebax matrix improves the permeability of CO_2 and selectivity of CO_2/CH_4 for 10% and 14%, respectively [17]. Amedi et al. studied Pebax-1657-based MMMs embedded with ZIF-8 particles which modified via (3-aminopropyl) trimethoxysilane (APTMS) and (3-aminopropyl) triethoxysilane (APTES). It is derived that the MMMs fabricated with modified ZIF-8 particles showed higher CO_2/CH_4 separation efficiency in comparison with the fabricated membranes with unmodified ZIF-8 [18]. Shamsabadi et al. modified TiO_2 nanoparticles with (3-aminopropyl) diethoxymethylsilane (APDEMS) and incorporated the amine-modified nanoparticles into Pebax-1657 matrix for the MMMs fabrication. The gas permeation studies showed that the surface modification improved both CO_2 permeability and CO_2/N_2 selectivity characteristics of the membranes [19]. Meshkat et al. fabricated MMMs via employing Pebax-1657 as the matrix and MIL-53 and surface-modified MIL-53 (NH_2-MIL-53) MOF as fillers to study the gas permeation characteristics of the prepared membranes. The results revealed that permeability of CO_2 and ideal CO_2/CH_4 and CO_2/N_2 selectivity values rose with adding both MIL-53 and NH_2-MIL-53, whereas the maximum CO_2 permeability was gained at 10 wt% loading of NH_2-MIL-53 with a 174% enhancement over that of the pristine Pebax membrane. Besides, at 10 wt% MIL-53, the ideal selectivity of CO_2/CH_4 and CO_2/N_2 was improved by 51% and 49%, respectively [1].

Although the idea of preparing Pebax-based MMMs has been considered for some time, based on the authors' studies, there is not any report of embedding the APTES-modified SiO_2 in the Pebax-1074 matrix to prepare MMMs for separation of CO_2/CH_4. Thus, the current work aims to study the CO_2/CH_4 separation features of Pebax-1074 membranes incorporated with the amine-modified SiO_2 nanoparticles and to specify the effect of their loading on the prepared membranes properties. The gas separation efficiency of the fabricated MMMs was studied via single gas permeation experiments. The distribution level of the nanofillers in the polymeric matrix, thermal properties, crystalline structure, and chemical bond variations of the prepared membranes were evaluated using FESEM, TGA, XRD, and FT-IR.

EXPERIMENTAL

1. Materials

Pebax®-1074, a thermoplastic elastomer that contains 45 wt% of the rigid polyamide 12 (PA-12) segments and 55 wt% of the flexible poly (ethylene oxide) (PEO) parts, was supplied from Arkema Inc. Hydrophilic and non-porous SiO_2 nanoparticles with 20-30 nm mean size, 2.4 $g \cdot cm^{-3}$ density, and 180-600 $m^2 \cdot g^{-1}$ specific area were purchased from US Research Nanomaterials, Inc. Methanol, n-hexane, toluene, and N, N-Dimethyl Formamide (DMF) solvents were purchased from Merck. APTES, which was employed for chemical modification of the nanoparticles with purity of 99.99%, was obtained from Sigma-Aldrich. The gases for the permeation experiments (CO_2 and CH_4) with purities of 99.99% and N_2 gas for the modification process were purchased from Farafan Gas Tehran Co.

2. Amine Modification of Nanoparticles

Nanoparticles have a robust propensity to experience agglomeration. Physical or chemical surface modifications of the metal oxide nanoparticles have been engaged to overcome the mentioned problem by decreasing the particle-particle interactions that reduce the agglomerates formation via reduction of physical forces [20]. SiO_2 nanoparticle modification with an amine agent was performed before their embedment into the Pebax matrix, for improving the separation properties of Pebax-1074/SiO_2 MMMs by enhancing their affinity to CO_2. Here, APTES was used as the coupling-agent of SiO_2 nanoparticles and Pebax, besides its role as the surface interaction enhancer with the polar gas (CO_2) molecules. To graft the reagent aminopropyl chains to the surface of SiO_2 nanoparticles, hydrolyzing the ethoxy groups is necessary at first [21,22]. The hydrolysis process was accomplished by dropwise addition of acidic water with pH=2 in APTES-methanol solution which had been exposed to magnetic stirring for 6 h. The amount of the employed acidic water and methanol was 3 and 2 moles based on the APTES mole, respectively. To accomplish the functionalization procedure, 5 g of the silica nanoparticles were distributed regularly in 120 ml pure toluene (anhydrous) with a probe-sonicator for 15 min. Then, the hydrolyzed APTES was poured into the prepared solution, and the mixture was stirred magnetically for 12 h at the ambient temperature under neutral N_2 atmosphere [17,21]. After that, the amine-modified SiO_2 nanoparticles (NH_2-SiO_2) were washed three times using ethanol to remove unreacted APTES and finally dried under a vacuum oven overnight. The amine-modification mechanism is depicted in Fig. 1.

3. Membrane Preparation

For removal of any possible adsorbed moisture, the elliptic pel-

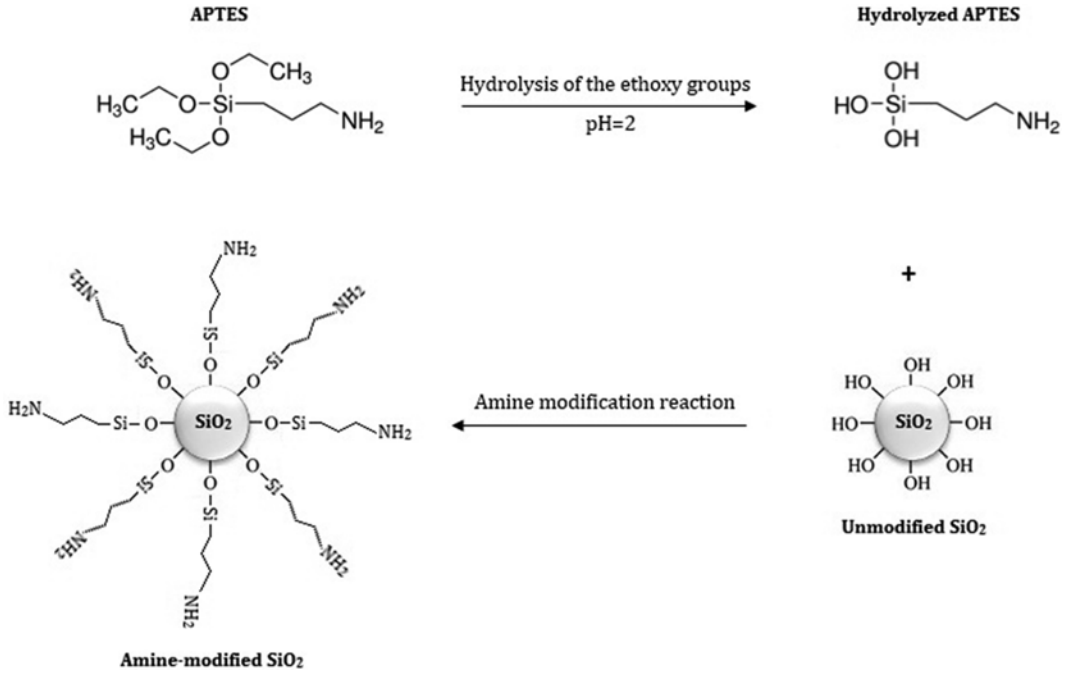

Fig. 1. Schematic representation of surface modification of SiO_2 nanoparticles with APTES.

lets of Pebax-1074 were located in a vacuum oven for 6 h at 80 °C. To prepare the neat membrane, a vessel of 2.5 wt% mixture of Pebax in DMF was placed in a glass oil container, and the obtained mixture was magnetically stirred at 110 °C for 3 h [23]. DMF was chosen as the solvent due to its near solubility parameter to that of the polymer, resulting in the formation of defect-free polymeric films. Furthermore, it can lead to high-speed gelation of the polymeric solution as it leaves the oil vessel and stays at room temperature, preventing nanoparticle agglomeration and sedimentation in the polymeric matrix during the drying process [24]. After complete dissolution of Pebax-1074 in the solvent, the obtained solution was poured into a Teflon Petri-dish of 7 cm diameter and put in the oven at 50 °C for 14 h. Finally, the pristine fabricated film was detached carefully from the dish and placed in a desiccator until use [24-26].

To prepare the MMMs, the mixture of specific content of NH_2-SiO_2 and pure SiO_2 nanoparticles (2.5, 5, 7.5, 10, 12.5 and 15 wt% based on the polymer mass) in DMF was fabricated and powerfully sonicated for about 30 min. For a more desirable interaction of Pebax-1074 and the SiO_2 nanoparticles, which can lead to the better distribution of the nanoparticles with lower aggregation, the temperature of the mixture was raised to the Pebax-1074 dissolution temperature (110 °C) gradually and then the elliptic pellets of Pebax-1074 were progressively added into the mixture, put under stirring in the glass oil container. Later, the same procedures for casting and drying were carried out for the pristine membrane [27,28]. The prepared membranes thicknesses were 50-60 μm which were measured by a digital micrometer.

4. Characterization

Fourier-transform infrared spectroscopy (FT-IR) was conducted by PerkinElmer spectrometer (Waltham, MA, USA) over the 400-4,400 cm^{-1} range to study the membranes and the nanoparticles functional groups and specify their chemical bonds alterations during the fabrication procedures.

The nanoparticle dispersion quality in the fabricated MMMs, as well as the membrane morphology, were studied via a Sigma, Zeiss field-emission scanning electron microscope (FESEM). For careful cross-sectional observation of the membranes, the synthesized films were broken cryogenically in N_2 liquid and then surface-coated with gold.

X-ray diffraction analysis (XRD) was accomplished using an INEL model EQUINOX 3000, France X-ray diffractometer furnished by Cu Kα X-radiation with 1.5406 Å wavelength over the 5-75° to explore crystallinity of the synthesized membranes during embedding nanoparticles into their matrices.

The thermal resistance of the fabricated membranes was examined via STA 504, BAHR thermal gravimeter with 10 °C/min heating rate under air atmosphere.

5. Gas Adsorption and Permeability Measurements

The pressure decline method was used to measure the isothermal adsorption of CO_2 and CH_4 gases on pure SiO_2 and NH_2-SiO_2 nanoparticles in a constant-volume cell at 25 °C over the 3-15 bar range. For measuring the pressure variations during the process of adsorption, the DMP 343 BD transmitter (accuracy of 1 mbar) was used, and the results were recorded by NX v.1.0.0. Before each test, the samples of nanoparticles were placed in a vacuum oven at 150 °C for 24 h to get rid of adsorbed moisture and gases. For conducting the tests, a definite quantity of the activated nanoparticles was located in the evacuated adsorption cell. The mentioned cell was then filled to a specified pressure by the intended gas via a sudden pulse. The adsorbed gas quantity on the SiO_2 nanoparticles was attained via the pressure decay technique and by an adequately accurate equation of state of Peng-Robinson was converted to moles. As the adsorption process was exceedingly temperature-

sensitive, an oven accommodating the adsorption cell was employed to provide the fixed temperature during the experiment [29].

For measuring pure gases (CO_2 and CH_4) permeation characteristics through the prepared membranes, a typical constant-volume system was employed [29]. The temperature of the feed gas could be constant as the membrane module was put in the oven, while the feed pressure was adjusted via a standard pressure regulator. The constant-volume approach was used to specify the pressure increase trend of a permeate gas at various feed pressures of 3, 6, 9, 12, and 15 bar and temperatures of 25, 35, 45, and 55 °C. The active membrane surface area was 10.45 cm^2. The gas permeability was calculated by the below equation:

$$P_i = \beta \times \frac{V \times l}{A \times T \times P_f} \times \left(\frac{dp}{dt}\right)_{s.s.} \quad (1)$$

where P_i is coefficient of component i permeability in Barrer (1 Barrer=10^{-10} cm^3 (STP) cm^{-1} s^{-1} $cmHg^{-1}$). β is a value used for unit conversion. V, l, A and T are representative of the chamber volume of the permeate side (cm^3), the thickness of the membrane (cm), effective area of the membrane (cm^2), and the feed temperature (K), respectively. The upstream pressure is designated by P_f (psia) and $\left(\frac{dp}{dt}\right)_{s.s.}$ is the diagram slope of the permeate gas pressure versus time as the steady state condition is achieved (mmHg s^{-1}) [26]. Note that the permeation experiments for any membrane sample were performed three times and the permeability coefficients were reported on average.

The value of ideal CO_2/CH_4 selectivity for each membrane can be calculated from pure gas permeability as shown below:

$$\alpha = \frac{P_{CO_2}}{P_{CH_4}} \quad (2)$$

where, P_{CO_2} and P_{CH_4} signify permeability values of gases CO_2 and

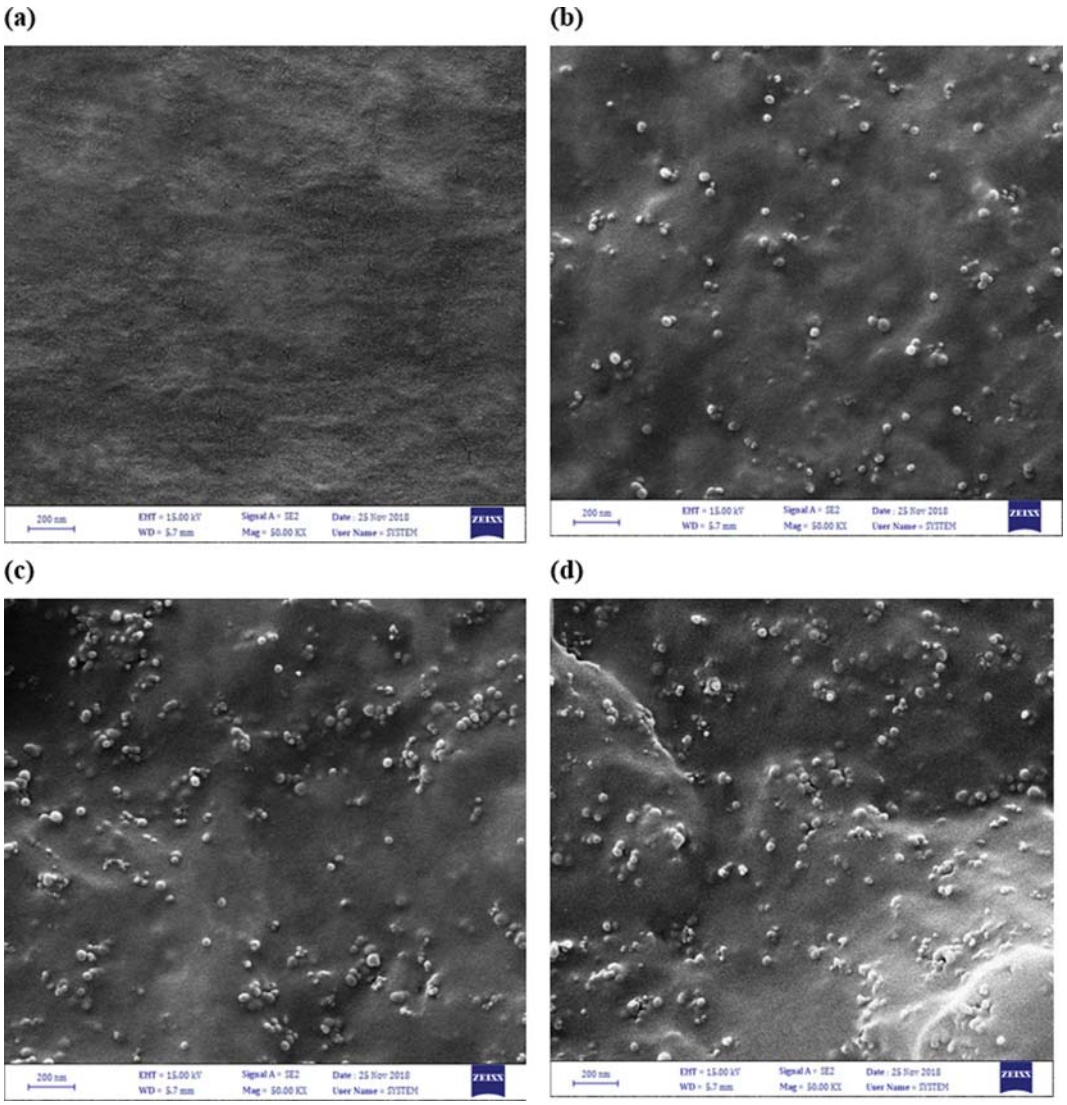

Fig. 2. FESEM cross-sectional images of (a) neat Pebax, (b) Pebax/NH_2-SiO_2 (2.5 wt%), (c) Pebax/NH_2-SiO_2 (5 wt%), (d) Pebax/NH_2-SiO_2 (7.5 wt%), (e) Pebax/NH_2-SiO_2 (10 wt%), (f) Pebax/NH_2-SiO_2 (12.5 wt%), and (g) Pebax/NH_2-SiO_2 (15 wt%) membranes.

CH_4, respectively [30].

RESULTS AND DISCUSSION

1. Morphological Analysis (FESEM)

A membrane separation characteristic mostly depends on its morphology and structure [27]. Fig. 2(a)-(g) shows a comparison of neat and MMMs FESEM cross-sectional images. As demonstrated in the figures, all the photographs display the lack of any defects and micro pores in the membranes structures, in addition to their dense structures. As can be seen in Fig. 2(b)-(f), in the cross-sectional photographs of MMMs incorporated with 2.5-12.5 wt% of NH_2-SiO_2, the nanoparticles were dispersed uniformly without any significant aggregation. In fact, the tendency of the NH_2-SiO_2 nanoparticles for accumulation and precipitation in the MMMs is minor owing to the employed powerful sonication, as well as the amine sites tendencies for interacting with the amide functional groups of the polymer through the hydrogen bonding, originating from the great amine groups basicity, which avoids the undesirable voids creation at the polymer-nanoparticles interface [17,28]. The FT-IR results can support these interactions between the polymer and the nanofillers. However, Fig. 2(g) displays that at the highest NH_2-SiO_2 nanoparticles loading (15 wt%), in comparison with the other loadings, some agglomeration is observed and the nanoparticles have a tendency to aggregate. In general, nanoparticle sedimentation, as well as their migration to the membrane surface, are two main reasons for their agglomeration. The sedimentation is due to the difference between the nanoparticles and the polymer densities, while the movement of the particle to the surface is owing to the membrane formation at a high temperature. If the nanoparticles are agglomerated in a polymer matrix, the gas permeation properties of the membrane may experience three undesirable things: (1) Formation of the non-selective voids at the polymer-nanoparticles interface, resulting in the MMM selectivity reduction. (2) Polymer chain rigidification which restricts the mobility of the polymer chains around the nanoparticles, reducing the

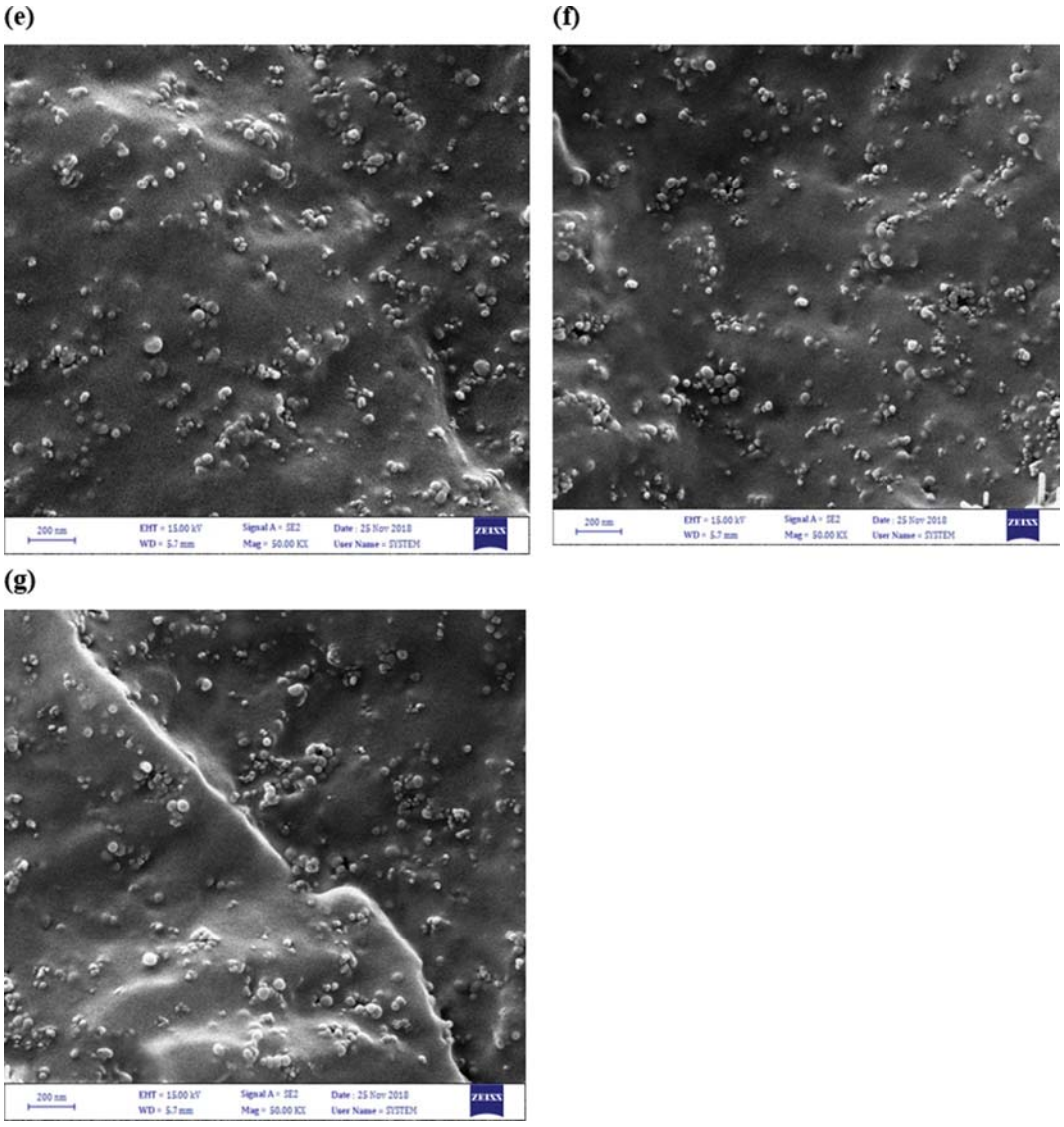

Fig. 2. Continued.

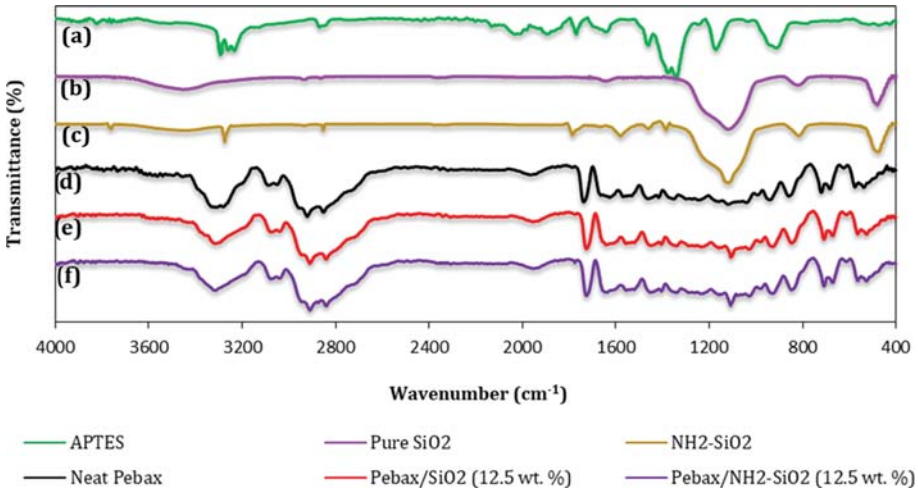

Fig. 3. FT-IR spectra of the pure SiO_2, amine-modified SiO_2 and the prepared membranes.

gas sorption, and accordingly its permeability through the MMM. (3) Sticking the nanoparticles and the creation of barriers for gas diffusion, decreasing the gas permeability through the MMM [31]. Here, by enhancing the nanofiller content more than 12.5 wt%, in the Pebax-1074 matrix, they agglomerated in the polymer matrix and subsequently created non-selective voids. It is expected that these cavities have adverse influences on the separation efficiency of the MMMs. It is notable that the previous research reveals that the unmodified SiO_2 agglomerates in the polymer matrix at the 12.5 wt% loading of the nanoparticles, which means the amine modification of the nanoparticles improves the stability and dispersion qualities of the amine-modified particles in the polymeric matrix of the membranes [17,23].

2. FT-IR Analysis

The pure and NH_2-SiO_2 nanofillers and the fabricated membranes were characterized by FT-IR analysis, as presented in Fig. 3. The characteristic peaks of the amine agent (APTES) signifying amine functional groups are bending vibrations of N-H group at 771 cm^{-1} and 1,575 cm^{-1}, as displayed in Fig. 3(a). Additionally, a weak peak at around 3,350 cm^{-1} is attributed to the stretching vibration of the NH_2 group [17]. In the IR spectrum of pure SiO_2 nanoparticles (Fig. 3(b)), the characteristic peaks at 480 and 1,118 cm^{-1} reflect the bending and stretching vibrations of the Si-O bond, respectively [29,32]. Moreover, the absorption peaks at 1,644 and 3,456 cm^{-1} specify the bending and stretching vibrations of the hydroxyl groups (OH) on the SiO_2 surface, respectively. Unlike pure SiO_2 nanoparticle spectrum, nearly the whole of APTES mentioned peaks are observed in the spectrum of NH_2-SiO_2 nanoparticles (Fig. 3(c)). However, the peaks of the NH_2 group of APTES cannot be recognized in the IR spectrum of the surface-modified particles as they overlap the peak related to the plentiful OH surface groups (3,456 cm^{-1}), but the reduction of OH peak strength for NH_2-SiO_2 can be an indication of substituting the OH groups with the amine functional groups [17]. Additionally, the observed peak assigned to Si-O-Si bond of NH_2-SiO_2 nanoparticles at 1,118 cm^{-1} displays the enhanced strength compared to pure SiO_2 spectrum (Fig. 3(b)), owing to the grafting the amino-silane groups on the silica particles surface [33]. For the pristine membrane (see Fig. 3(d)), a characteristic peak at 1,112 cm^{-1} is assigned to the ether group of the PE part symmetric vibration [34-36]. Furthermore, the existence of the bonded and free carbonyl in H-N-C=O is proved regarding the observed peaks at wavenumbers of 1,626 and 1,636 cm^{-1}, respectively. Moreover, a peak at 1,734 cm^{-1} is related to the presence of the O-C=O group in the PA part [37]. The characteristic peaks related to the N-H free and bonded bending vibrations are observed at 1,548 and 1,564 cm^{-1}, while those contribute to the free and bonded stretching vibrations of the N-H group can be seen at 3,290 and 3,328 cm^{-1}, respectively [38,39]. The pristine membrane spectrum reveals two observed peaks at 1,460 and 2,922 cm^{-1}, which are indicative of the aliphatic -C-H bond stretching and bending vibrations, respectively. A broad observed peak located at 3,400-3,700 cm^{-1} is assigned to OH groups, which signifies the hydrogen bonding among the PA segments of the Pebax [34,37, 40,41]. Embedding the SiO_2 nanoparticles (both pure SiO_2 and NH_2-SiO_2) in the polymer matrix may cause some alterations in the position and strength of their IR spectra characteristic peaks in comparison with the pristine membrane, because of the polymer-nanoparticles interactions. To observe these changes, the MMM incorporated with 12.5 wt% of pure SiO_2, as well as that of with the highest separation performance (Pebax/NH_2-SiO_2 loaded with 12.5 wt% of NH_2-SiO_2), were chosen for the comparison of their IR spectra with that of the pristine Pebax membrane. As seen in their IR spectra (Fig. 3(e) and (f)), in the 1,100-1,200 cm^{-1} range, the Si-O-Si characteristic peak of the SiO_2 nanofillers can be observed in their polymeric matrix. It can be clearly understood that some characteristic peak intensities of the neat membrane decreased and were shifted to higher frequencies in the MMMs spectra due to the existence of SiO_2 nanoparticles. As an example, in the neat membrane IR spectrum, the peaks at 1,626 and 1,636 cm^{-1}, signifying the bonded and free C=O group of the PA, represent that PA segments are connected by hydrogen bonding. The embedment of SiO_2 nanofillers into the polymer matrix has caused the observed peak of the free C=O to disappear, and MMMs peaks representing the bounded C=O groups be shifted to higher frequencies. Moreover, as shown in Fig. 3(e) and (f), a substantial variation in the N-H stretching vibration occurred. The enhanced loading of

SiO_2 nanoparticles led the peak intensity of the free N-H to be weakened considerably, and the hydrogen-bonded N-H stretching peaks shifted to higher wavenumbers. The mentioned variations in the MMMs spectra can be a sign of the rupture of hydrogen bonding among the PA segments of Pebax, which consequently resulted in the crystallinity reduction of the Pebax-1074 matrix as it will be confirmed by XRD results. Additionally, a great decrease in the peak strength of OH at 3,400-3,600 cm^{-1} was detected, in comparison with the pristine Pebax membrane spectrum [42]. The NH_2 group of NH_2-SiO_2 surface could be detected directly in the MMMs IR spectra owing to the existence of plentiful OH groups in the same frequencies. However, comparison of the IR spectra of the MMMs loaded with pure and NH_2-SiO_2 nanoparticles reveals that there is a greater peak of aliphatic amine at near 2,880 cm^{-1} in the Pebax/NH_2-SiO_2 12.5 wt% MMM spectrum, representing the amine-functionalized nanoparticles existence in its polymeric matrix (see Fig. 3(e) and (f)) [17,18].

3. XRD Analysis

X-ray diffraction (XRD) analysis patterns of the pristine Pebax and the MMMs are displayed in Fig. 4. The XRD pattern of the Pebax-based membrane contains strong and weak diffraction peaks at around 22 and 11 of 2θ, respectively, which contribute to crystalline and amorphous regions, respectively, confirming the semi-crystalline polymer structure. As mentioned, Pebax comprises hard PA and soft PE blocks, which causes the formation of the semi-crystalline structure of the polymer [42,43]. It is observable that for the MMMs, the incorporation of NH_2-SiO_2 nanoparticles into the Pebax matrix reduces the strength of the characteristic peaks of the polymer, and with enhancing the nanoparticles content up to 12.5 wt%, this influence increases. This behavior shows the existence of SiO_2 nanoparticles leads the total membrane crystallinity to be reduced, and the amorphous phase raised because the hydrogen bonds among the PA segments of the polymer are disrupted, as proved by the FT-IR results. Besides, d-spacing which is representative of molecular distance among polymer chains, is oppositely relative to the position of crystalline peaks (2θ) as described by the Bragg equation, ($n\lambda=2d\sin\theta$) [44-46]. Extra studies on the XRD patterns revealed that via enhancing the loading from 0 to 12.5 wt%, the crystalline region diffraction peaks of the polymer were slightly shifted to lower degrees from 22.3 to 21.7 of 2θ,

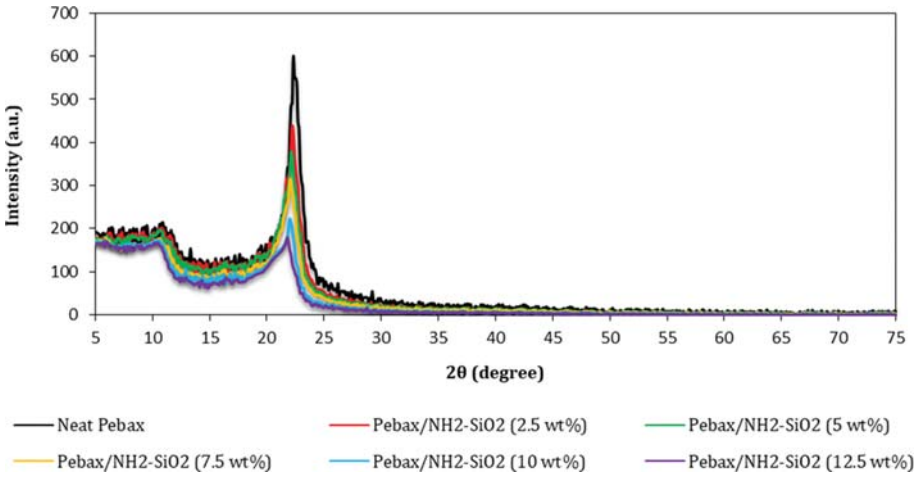

Fig. 4. XRD patterns of the prepared membranes.

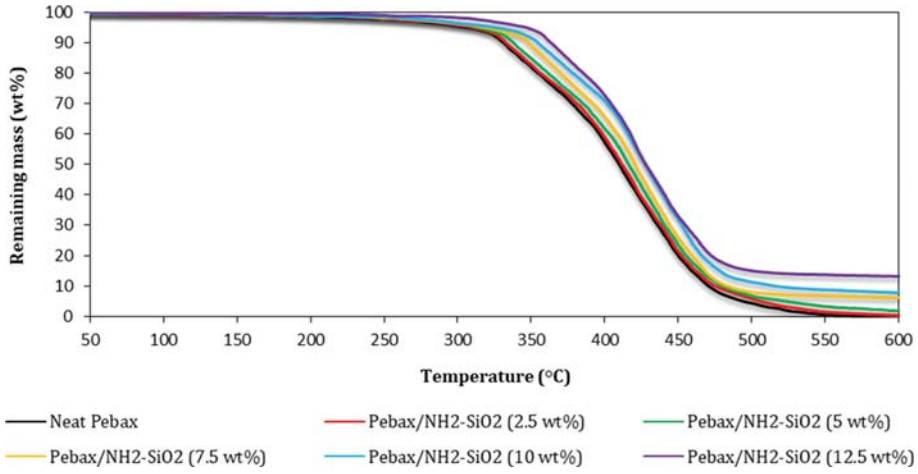

Fig. 5. TGA curves of the prepared membranes.

which are attributed to an increase of the d-spacing parameter from 3.98 to 4.09 Å. These changes signify a rise in the intersegment distance of Pebax chains, which can result in more fractional free volume (FFV), as well as the higher polymer amorphous nature. Consequently, gas permeability of the MMMs membranes is anticipated to be improved, regarding the reduction of the polymer crystallinity, as well as the increase of intersegment distances and FFV [27,29].

4. Thermal Stability Analysis

To investigate the effect of SiO_2 nanoparticles on the thermal resistance of prepared MMMs, thermal gravimetric analysis was conducted for the pristine membrane and the MMMs. The thermal resistance of the membranes in terms of the remaining polymer weight (wt%) with the temperature increase was demonstrated in Fig. 5. As depicted in Fig. 5, the thermal degradation of the membranes takes place in the three following steps. The first step for the neat membrane from 50 to 320 °C shows the residual solvent, as well as the probable adsorbed water evaporation, whereas the next step from 320 to 480 °C expresses the principal degradation, which signifies decomposing the polymer chains. The third step beginning at 480 °C exhibits carbonization of the thermal degraded Pebax chains [27]. The mentioned steps for the MMMs occur at different temperature limits. The results display that the addition of SiO_2 nanoparticles into the polymer matrix increased the thermal stability of the MMMs in comparison with the pristine Pebax membrane. Thus, the thermal resistance of the membranes increases as the nanoparticles are introduced into the polymer matrix, leading at great operating temperatures the membranes not to degrade. For example, the main degradation temperature for the pristine membrane is at about 400 °C, while it is almost at 405, 410, 416, 420 and 422 °C for the MMMs incorporated with 2.5, 5, 7.5, 10 and 12.5 wt%, respectively. These enhancements can be assigned to thermal barriers caused by the existence of highly thermal resistant nanoparticles in the Pebax matrix [47-49].

5. Gas Adsorption Efficiency of Nanoparticles

The adsorption isotherms of CO_2 and CH_4 for both pure and NH_2-SiO_2 nanoparticles are displayed in Fig. 6. The nanoparticle adsorption capability is influenced by the properties of adsorbed gas molecules and functional groups on nanoparticles surfaces, as well. As shown in Fig. 6, for both pure and NH_2-SiO_2 nanoparticles, the adsorbed CO_2 amount is more than that of CH_4, as the CO_2 molecules of dipole moment tend to interact with functional groups of the nanoparticles more than non-polar molecules (CH_4). Low amount of adsorbed CH_4 is due to the symmetric vibrations, which were temporarily causing the polarity and led CH_4 molecules to be apt for a slight interaction with the functional groups existing on the particles surfaces [50,51]. The functional group kind is the main parameter for gas adsorption characteristics of particles, as mentioned previously. Study of both gases adsorption isotherms showed that CO_2 molecules could be adsorbed higher on NH_2-SiO_2 nanoparticles compared to the unmodified nanoparticles because of the nucleophile reactions between the CO_2 molecules and NH_2 functional groups, which is significantly stronger and more effective than the gas molecule reaction with OH groups [17,52]. The reaction reversibility indicates that CO_2 molecules can detach the nanoparticle surfaces in the process owing to the carbonate compound instability. Moreover, the adsorption isotherms, shown in Fig. 6, demonstrate that by enhancing the pressure from 3 to 15 bar, CO_2 adsorption quantity will increase for both nanofillers. The adsorbed CO_2 gas amount for the unmodified nanoparticles was 0.015 mmol·g^{-1} at the pressure of 3 bar and reached 0.040 mmol·g^{-1} when the pressure rose to 15 bar, while these amounts for NH_2-SiO_2 nanoparticles increased after the modification and led to the sharp increase in CO_2 adsorption capacity from 0.021 to 0.092 mmol·g^{-1}. In both isotherms, a small enhancement of CO_2 adsorption capacity at the pressure variation from 12 to 15 bar showed that they get close to reach their maximum adsorption capacities at the equilibrium state [53-55].

6. Gas Permeation Properties

6-1. The Nanoparticle Loading Effect

The pure SiO_2 and NH_2-SiO_2 nanoparticle loading influences CO_2 and CH_4 can be observed in Figs. 7(a) and (b) at the pressure

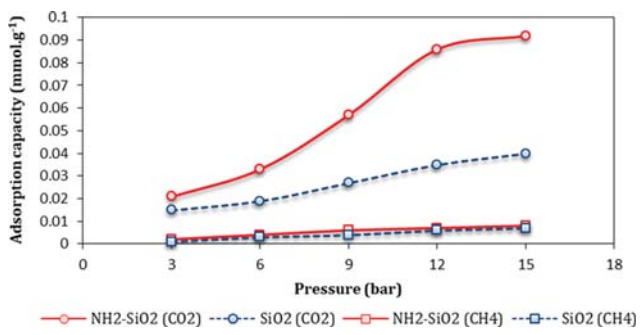

Fig. 6. CO_2 and CH_4 adsorption capacity of pure and amine-modified SiO_2 nanoparticles.

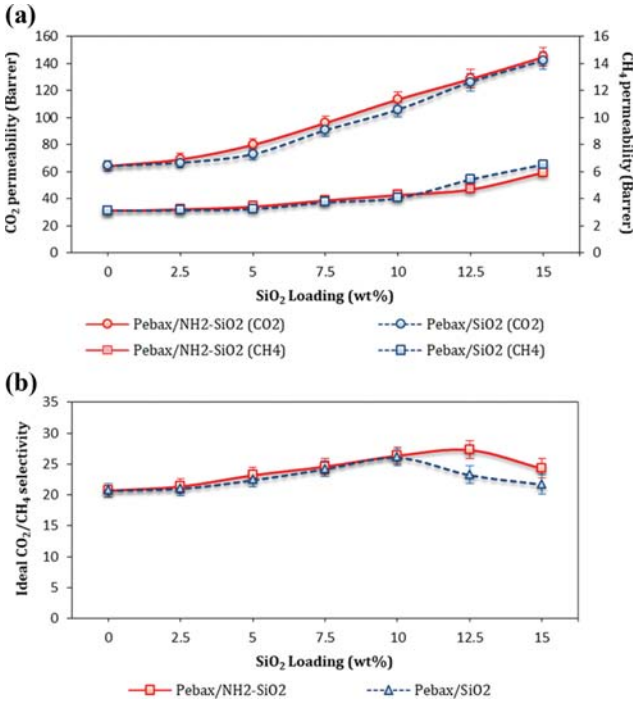

Fig. 7. Influence of the SiO_2 content on (a) CO_2 and CH_4 permeabilities, and (b) ideal CO_2/CH_4 selectivity.

and the temperature of 3 bar and 25 °C, respectively. As depicted in Fig. 7(a), as the nanoparticle (both pure SiO_2 and NH_2-SiO_2) loading rises from 0 to 12.5 wt%, CO_2 permeability quantities through MMMs containing pure-SiO_2 and NH_2-SiO_2 particles increase from 64.51 to 126.42 and 128.89 Barrer, respectively, whereas CH_4 permeability increases from 3.11 to 5.43 and 4.72 Barrer, respectively. This permeation increment is because of the polymer crystallinity reduction, the FFV increase, as well as the chain mobility in the existence of the nanofillers, as was approved by the XRD and FT-IR results [34]. As observed, embedding SiO_2 nanoparticles into the polymer matrix caused a remarkable rise of CO_2 permeability and a slight growth of CH_4 permeability through MMMs. This behavior can be ascribed to the greater affinity of CO_2 to SiO_2 nanoparticles compared to that of CH_4 to the particles and creation of selective voids at the interface of polymer-nanoparticles, as well the inconsistency of the polymer matrix and the nanoparticles. However, the CO_2 permeability through the MMMs composed of NH_2-SiO_2 increases more than those containing pure SiO_2 nanoparticles, as the nanofillers content rises in the polymer matrix. This can be described by the fact that the CO_2 molecules interact with the amine functional groups of amine-modified SiO_2 more than OH groups of pure SiO_2 nanoparticles, which causes the MMMs loaded with NH_2-SiO_2 to have the higher CO_2 solubility and accordingly permeability compared to the membranes embedded with pure SiO_2 of the same loading. The reactive amine sites with electrons provide nitrogen as a Lewis base anterior of CO_2 molecules. The reactions of CO_2 molecules with amine functional groups is as follows [52]:

$$CO_2+RNH_2 \leftrightarrow RNH_2+COO^- \quad (3)$$

$$2RNH_2+COO^- \leftrightarrow RNH_3^+ + RNHCOO^- \quad (4)$$

where a CO_2 molecule can react with the propylamine group at first to produce carbamic acid, and then the product will react with a different free amine group, producing a carbamate molecule and RNH_3^+ [52]. As noted earlier, due to the reversibility of the reactions and instability of carbonate compounds, the CO_2 molecules may be desorbed completely from the nanoparticle surfaces. This phenomenon was not seen for permeability of CH_4 since the non-polar gas did not show a remarkable interaction with NH_2 and OH groups.

As observed in Fig. 7(c), with enhancing the pure SiO_2 nanoparticles loading up to 10 wt%, the ideal CO_2/CH_4 selectivity rises from 20.74 to 26.09 because the CO_2 permeability increment is more than that of CH_4, resulting from greater CO_2 affinity to SiO_2 nanoparticles, as well as the selective void formation [56-58]. However, as the SiO_2 nanoparticles increase from 10 to 15 wt%, the ideal CO_2/CH_4 selectivity declines from 26.09 to 21.76. The main reason for this behavior is that SiO_2 nanoparticles agglomerate in the Pebax matrix undesirably, resulting in the creation of non-selective voids and accordingly CH_4 molecules can permeate higher than when the nanoparticles loading is lower than 10 wt%. For MMMs containing amine-modified SiO_2, the ideal selectivity increases to 27.31 as the nanoparticles loading increases up to 12.5 wt% and then decreases to 24.30 with further loading of the nanoparticles in the Pebax matrix. Actually, amine (APTES) modification of the nanoparticles improved the nanoparticles CO_2 adsorption capacity, as well as their better dispersion into the Pebax matrix due to the improved interfacial compatibility of the nanofillers and the Pebax, resulting in increasing the polymer matrix capacity for higher embedment of NH_2-SiO_2 than pure SiO_2. This leads to the higher separation performance of MMMs loaded with amine-modified SiO_2 particles compared to those incorporated with pure SiO_2 particles [17,19].

6-2. The Feed Pressure Effect

Figs. 8(a), (b) and (c) display the various feed pressure effects on the CH_4 and CO_2 gases permeability and CO_2/CH_4 selectivity values of the fabricated membranes at the constant temperature of 25 °C. Regarding to the results, by improving the feed pressure from 3 to 15 bar, both CH_4 and CO_2 permeability values increased due to the increased gas transfer driving force through the prepared membranes [5,37,46]. However, the CO_2 permeability in-

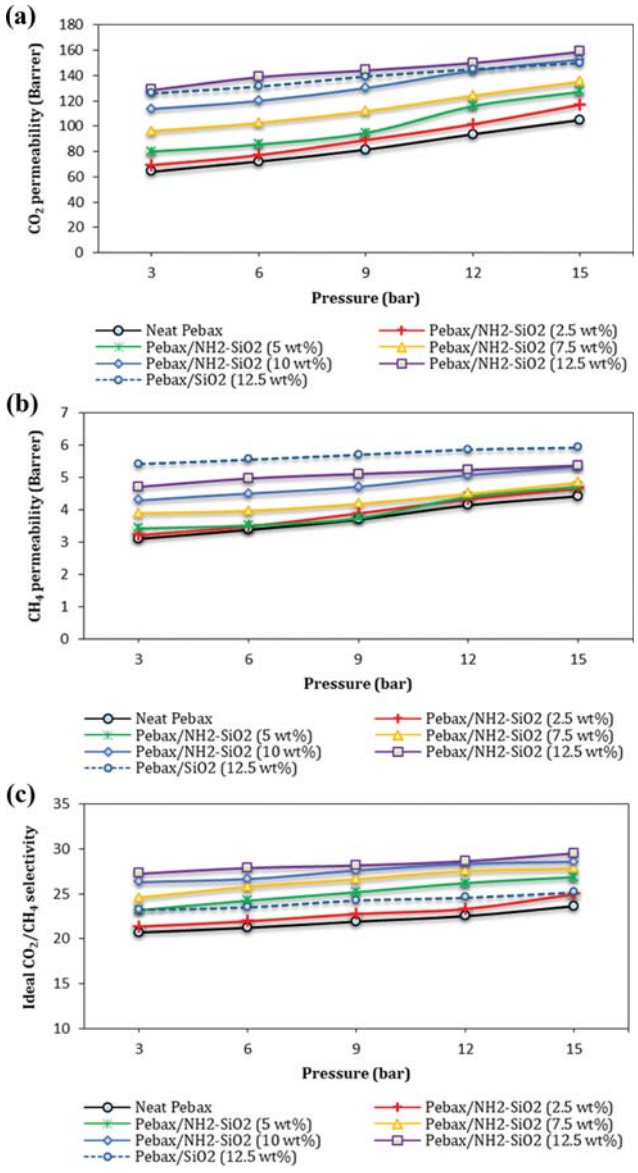

Fig. 8. Influence of the feed pressure on (a) CO_2 permeability, (b) CH_4 permeability and (c) ideal CO_2/CH_4 selectivity.

creased considerably, while the CH_4 permeability increased slightly. A rubbery membrane solubility parameter depends on a gas condensability feature. Since the critical temperatures of CO_2 and CH_4 are 31.1 and −82.3 °C, respectively, the condensable CO_2 gas permeability increases higher in comparison with the non-condensable gas (CH_4) permeability. In fact, CO_2 molecules have a higher affinity for the PE blocks of the polymer in comparison with CH_4. Besides, CO_2 is apt to plasticize the Pebax matrix because it is an acidic gas which will result in improving CO_2 permeability higher than that of CH_4 when the pressure rises [41,59]. Therefore, ideal CO_2/CH_4 selectivity experiences a rising trend as the pressure rises from 3 to 15 bar. For example, the ideal CO_2/CH_4 selectivity of the pristine membrane is enhanced from 20.74 to 23.69, whereas that of the MMM embedded with 12.5 wt% of the pure SiO_2 from 23.28 to 25.24 and that of the MMM incorporated with 12.5 wt% of the NH_2-SiO_2 from 27.30 to 29.57. One can observe that the increase of CO_2 permeability for the MMMs incorporated with NH_2-SiO_2 is more than the MMMs incorporated with pure SiO_2, and for those incorporated with pure SiO_2 is more than the neat membrane. The principal reason for this is that the CO_2 adsorption capacity of the NH_2-SiO_2 nanofillers increases more as the feed pressure increases [29].

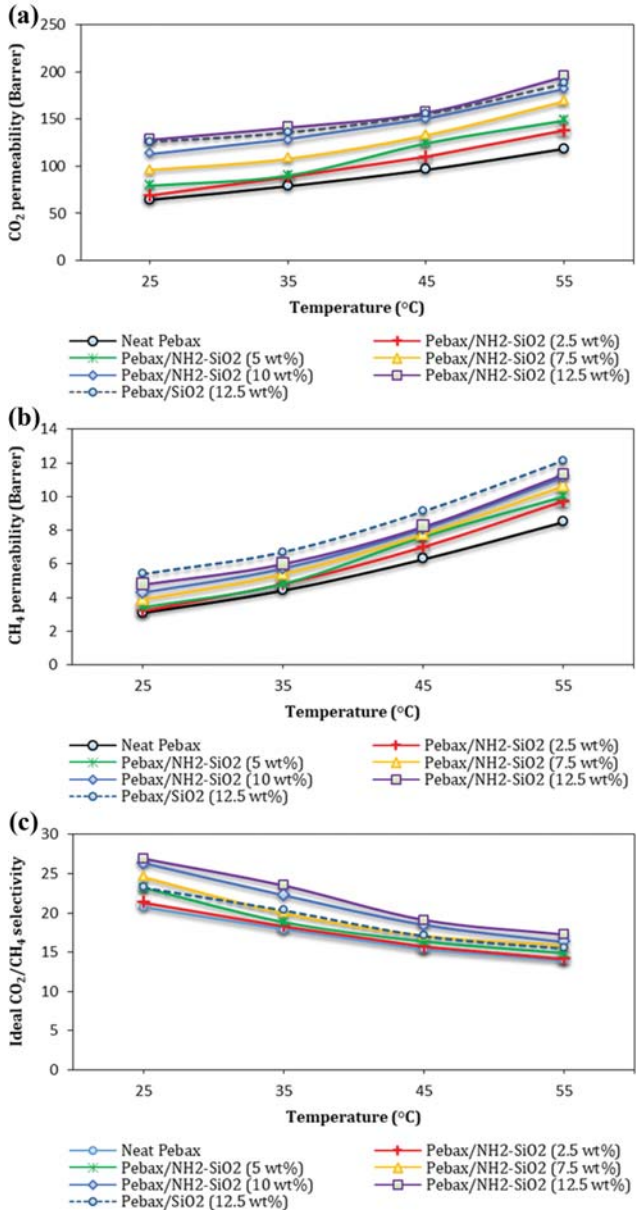

Fig. 9. Influence of the feed temperature on (a) CO_2 permeability, (b) CH_4 permeability and (c) ideal CO_2/CH_4 selectivity.

6-3. The Feed Temperature Effect

Figs. 9(a), (b) and (c) show the effects of temperature changes on CH_4 and CO_2 gases permeability and CO_2/CH_4 selectivity values of the fabricated membranes at 3 bar. As shown in Figs. 9(a) and (b), by enhancing the operating temperature from 25 to 55 °C, the permeability of CH_4 and CO_2 gases through all the prepared membranes increased due to the increase of polymer chains movements [25]. For instance, for the MMM incorporated with 12.5 wt% of NH_2-SiO_2 nanofillers, the permeability of CO_2 increased from 128.89 to 195.76 Barrer, whereas this feature for CH_4 was changed from 4.79 to 11.35 Barrer. As can be seen, the temperature effect on the permeability of CH_4 is greater than that of CO_2. As a result, which can be displayed in Fig. 9(c), the ideal CO_2/CH_4 selectivity of the membranes decreased by the temperature growth. For better clarification of this behavior, it is vital to investigate the equation of van't Hoff-Arrhenius (Eq. (3)), expressing the temperature dependence of a penetrant through a polymeric dense membrane [5,60]:

$$P = P_0 \exp\left(\frac{-E_p}{RT}\right) \quad (5)$$

where P_0, E_p, T, and R are the pre-exponential factor (Barrer), the permeation apparent activation energy (J mol^{-1}), the temperature (K) and the gas constant, respectively. By the mentioned equation, the activation energy (E_p) can be obtained from the line slope of Ln P versus 1/T. Consequently, E_p of the gas of lower permeability (CH_4) is greater compared to that of higher permeability (CO_2) [37]. This signifies that the CH_4 temperature sensitivity is higher than that of CO_2. Thus, the temperature rise influence on the CH_4 permeability is higher than that of CO_2, causing the membrane ideal CO_2/CH_4 selectivity to be reduced by raising the operating temperature [37]. As an example, as the temperature of feed rose from 25 to 55 °C, the pristine membrane CO_2/CH_4 selectivity decreased from 20.74 to 13.97, whereas that of the MMM embedded with 12.5 wt% of the pure SiO_2 from 23.28 to 15.53 and that of the MMM incorporated with 12.5 wt% of the NH_2-SiO_2 from 26.91 to 17.25.

6-4. The Membrane Performance Data on Robeson's Diagram

To further study the effect of incorporated amine-modified SiO_2 nanoparticles on CO_2 and CH_4 gases permeation characteristics of the synthesized membranes and also compare the efficiency of the MMMs (Pebax-1074/SiO_2 and Pebax-1074/NH_2-SiO_2) with the upper bound limits of Robeson's diagram, their data points at 25 °C and 3 bar were positioned on the plot of CO_2/CH_4 selectivity-CO_2 permeability (Robeson's diagram) (see Fig. 10). Most of the researches on gas separation membranes aim to get nearer to the Robeson upper bound lines or cross the bounds, being first offered in 1991 [61] and revisited in 2008 [62]. As displayed in Fig. 10, by enhanc-

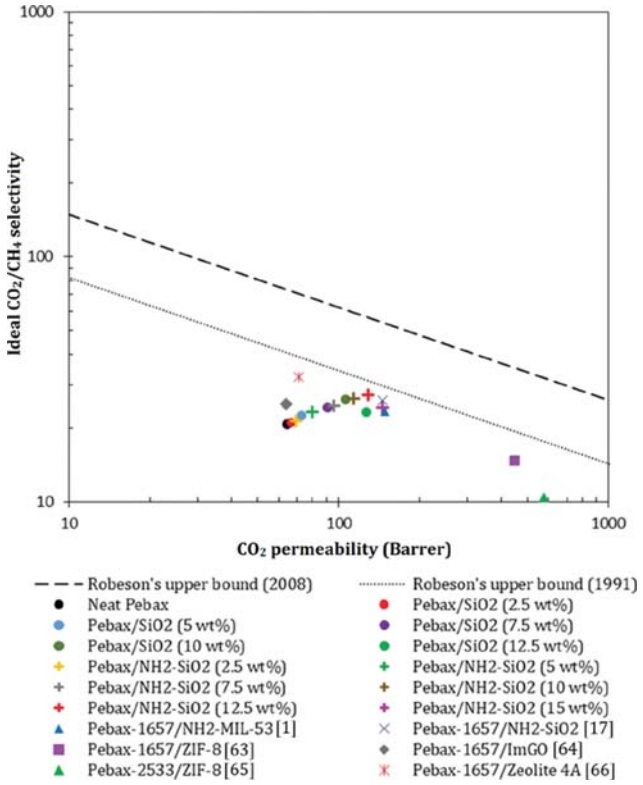

Fig. 10. CO_2/CH_4 separation efficiency of various Pebax-based MMMs compared to Robeson's upper bounds.

ing pure SiO_2 nanoparticle content up to 10 wt%, the performance of membranes (CO_2/CH_4 selectivity, in addition to CO_2 permeability) increases and accordingly the membranes selectivity-permeability data get closer to the bounds. However, with the further rise of the nanoparticle content up to 12.5 wt%, CO_2 permeability increases, whereas the selectivity decreases and the data points being distanced from 1991 bound. Moreover, as NH_2-SiO_2 nanoparticle content increases from 0 to 12.5 wt%, both CO_2 permeability and ideal CO_2/CH_4 selectivity are enhanced, and consequently, the corresponding membranes data get closer to the Robeson lines. However, additionally raising the NH_2-SiO_2 nanofillers content distances the membrane data points from the Robeson upper bound because the membrane CO_2/CH_4 selectivity is reduced.

Besides, the efficiency of some Pebax-based MMMs, which has been stated in the literature, is displayed in Fig. 10 [1,17,63-66]. As shown, the data point coordinate of the MMM loaded with 12.5 wt% of NH_2-SiO_2 nanofillers is closer to 1991 bound compared to other membranes data points. Accordingly, the fabricated membranes in the current study can be considered suitable choices for CO_2/CH_4 separation.

CONCLUSION

The Pebax-1074 based MMMs were prepared by incorporating SiO_2 and its amine-functionalized counterpart (NH_2-SiO_2) into the polymer matrix. FESEM micrographs revealed a more uniform dispersion of NH_2-SiO_2 compared to pure SiO_2 nanoparticle into Pebax matrix, as well as an acceptable NH_2-SiO_2 dispersion at loadings lower than 12.5 wt%; however, at the maximum loading (15 wt%) the nanoparticles tended to be aggregated in the Pebax matrix. TGA results showed enough stability of the prepared membranes for traditional gas separation applications and also confirmed the increase in the thermal resistance of the membrane, as the nanoparticles loading rose in the polymer matrix. FT-IR spectroscopy confirmed the effective amine modification of SiO_2 nanoparticles, as well as hydrogen bonding disruption among the PA segments by the nanofillers addition, resulting in the increased gases permeations. XRD results were in good agreement with those of FT-IR and showed membrane crystallinity reduction and accordingly the membrane FFV enhancement, by increasing the nanoparticles loading. Gas permeation experiments showed promising results for CO_2 permeability and CO_2/CH_4 selectivity of either Pebax-1074/NH_2-SiO_2 or Pebax-1074/SiO_2 membranes. The greater capacity of the SiO_2 nanoparticles for CO_2 adsorption, as well as the selective voids creation at the SiO_2-Pebax interface, clearly justify the SiO_2 contribution to improving the MMMs gas separation efficiencies. The gas permeation experiments also revealed that amine modification of the nanoparticles before being added into the Pebax matrix raises CO_2 permeability and accordingly ideal CO_2/CH_4 selectivity, resulting from the enhanced CO_2 adsorption capability of the nanofillers after amine functionalization.

REFERENCES

1. S. Meshkat, S. Kaliaguine and D. Rodrigue, *Sep. Purif. Technol.*, **200**, 177 (2018).
2. N. Azizi and M. R. Hojjati, *Pet. Sci. Technol.*, **36**, 993 (2018).
3. N. Azizi and M. M. Zarei, *Pet. Sci. Technol.*, **35**, 869 (2017).
4. H. Rajati, A. H. Navarchian and S. Tangestaninejad, *Chem. Eng. Sci.*, **185**, 92 (2018).
5. H. Rabiee, S. Meshkat Alsadat, M. Soltanieh, S. A. Mousavi and A. Ghadimi, *J. Ind. Eng. Chem.*, **27**, 223 (2015).
6. A. Ghadimi, T. Mohammadi and N. Kasiri, *Int. J. Hydrogen Energy*, **40**, 9723 (2015).
7. A. Ghadimi, S. Norouzbahari, M. Sadrzadeh and T. Mohammadi, *Polym. Adv. Technol.*, **23**, 1101 (2012).
8. M. Asghari, M. Mosadegh and H. R. Harami, *Chem. Eng. Sci.*, **187**, 67 (2018).
9. A. Moghadassi, Z. Rajabi, S. Hosseini and M. Mohammadi, *Sep. Sci. Technol.*, **48**, 1261 (2013).
10. P. Goh, A. Ismail, S. Sanip, B. Ng and M. Aziz, *Sep. Purif. Technol.*, **81**, 243 (2011).
11. S. Hwang, W. S. Chi, S. J. Lee, S. H. Im, J. H. Kim and J. Kim, *J. Membr. Sci.*, **480**, 11 (2015).
12. M. Khajouei, M. Peyravi and M. Jahanshahi, *J. Membr. Sci. Res.*, **3**, 2 (2017).
13. E. Ataeivarjovi, Z. Tang and J. Chen, *ACS Appl. Mater. Interfaces*, **10**, 28992 (2018).
14. M. Sadeghi, M. Mehdi Talakesh, B. Ghalei and M. Shafiei, *J. Membr. Sci.*, **427**, 21 (2013).
15. S. Hassanajili, M. Khademi and P. Keshavarz, *J. Membr. Sci.*, **453**, 369 (2014).
16. M. Rezakazemi, A. Vatani and T. Mohammadi, *RSC Adv.*, **5**, 82460

(2015).
17. M. Isanejad and T. Mohammadi, *Mater. Chem. Phys.*, **205**, 303 (2018).
18. H. R. Amedi and M. Aghajani, *Micropor. Mesopor. Mater.*, **247**, 124 (2017).
19. A. A. Shamsabadi, F. Seidi, E. Salehi, M. Nozari, A. Rahimpour and M. Soroush, *J. Mater. Chem. A*, **5**, 4011 (2017).
20. S. Mallakpour and M. Madani, *Prog. Org. Coat.*, **86**, 194 (2015).
21. E. Bourgeat-Lami, P. Espiard and A. Guyot, *Polymer*, **36**, 4385 (1995).
22. R. Antony, S. T. D. Manickam, P. Kollu, P. Chandrasekar, K. Karuppasamy and S. Balakumar, *RSC Adv.*, **4**, 24820 (2014).
23. S. Azizi, N. Azizi and R. Homayoon, *Silicon*, **11**, 2045 (2019).
24. M. Isanejad, N. Azizi and T. Mohammadi, *J. Appl. Polym. Sci.*, **134**, 44531 (2017).
25. N. Azizi, M. Arzani, H. R. Mahdavi and T. Mohammadi, *Korean J. Chem. Eng.*, **34**, 2459 (2017).
26. A. Ghadimi, T. Mohammadi and N. Kasiri, *Ind. Eng. Chem. Res.*, **53**, 17476 (2014).
27. N. Azizi, T. Mohammadi and R. M. Behbahani, *J. Energy Chem.*, **26**, 454 (2017).
28. N. Azizi, T. Mohammadi and R. M. Behbahani, *J. Nat. Gas Sci. Eng.*, **37**, 39 (2017).
29. N. Azizi, T. Mohammadi and R. Mosayebi Behbahani, *Chem. Eng. Res. Des.*, **117**, 177 (2017).
30. F. Moghadam, M. R. Omidkhah, E. Vasheghani-Farahani, M. Z. Pedram and F. Dorosti, *Sep. Purif. Technol.*, **77**, 128 (2011).
31. M. Rezakazemi, A. E. Amooghin, M. M. Montazer-Rahmati, A. F. Ismail and T. Matsuura, *Prog. Polym. Sci.*, **39**, 817 (2014).
32. J. H. Chen, M. Z. Rong, W. H. Ruan and M. Q. Zhang, *Compos. Sci. Technol.*, **69**, 252 (2009).
33. A. D'Agostino, M. E. Errico, M. Malinconico, M. De Rosa, M. Avella and C. Schiraldi, *J. Mater. Sci.: Mater. Med.*, **22**, 481 (2011).
34. J. H. Kim and Y. M. Lee, *J. Membr. Sci.*, **193**, 209 (2001).
35. M. C. Choi, J. Y. Jung, H. S. Yeom and Y. W. Chang, *Polym. Eng. Sci.*, **53**, 982 (2013).
36. H. R. Mahdavi, N. Azizi, M. Arzani and T. Mohammadi, *J. Nat. Gas Sci. Eng.*, **46**, 275 (2017).
37. A. Ghadimi, M. Amirilargani, T. Mohammadi, N. Kasiri and B. Sadatnia, *J. Membr. Sci.*, **458**, 14 (2014).
38. D. Dixon and A. Boyd, *Polym. Eng. Sci.*, **51**, 2203 (2011).
39. Y. Wang, J. Ren and M. Deng, *Sep. Purif. Technol.*, **77**, 46 (2011).
40. R. S. Murali, K. P. Kumar, A. Ismail and S. Sridhar, *Micropor. Mesopor. Mater.*, **197**, 291 (2014).
41. H. Rabiee, A. Ghadimi and S. Abbasi, *Chem. Eng. Res. Des.*, **98**, 96 (2015).
42. R. S. Murali, S. Sridhar, T. Sankarshana and Y. Ravikumar, *Ind. Eng. Chem. Res.*, **49**, 6530 (2010).
43. Y. Yampolskii and B. Freeman, *Membrane gas separation*, Wiley Online Library (2010).
44. R. Surya Murali, A. F. Ismail, M. A. Rahman and S. Sridhar, *Sep. Purif. Technol.*, **129**, 1 (2014).
45. D. Zhao, J. Ren, H. Li, X. Li and M. Deng, *J. Membr. Sci.*, **467**, 41 (2014).
46. S. Wang, Y. Liu, S. Huang, H. Wu, Y. Li, Z. Tian and Z. Jiang, *J. Membr. Sci.*, **460**, 62 (2014).
47. N. A. H. M. Nordin, S. M. Racha, T. Matsuura, N. Misdan, N. A. A. Sani, A. F. Ismail and A. Mustafa, *RSC Adv.*, **5**, 43110 (2015).
48. N. A. H. M. Nordin, A. F. Ismail, A. Mustafa, R. S. Murali and T. Matsuura, *RSC Adv.*, **5**, 30206 (2015).
49. F. Dorosti, M. Omidkhah and R. Abedini, *J. Nat. Gas Sci. Eng.*, **25**, 88 (2015).
50. P. Chowdhury, S. Mekala, F. Dreisbach and S. Gumma, *Micropor. Mesopor. Mater.*, **152**, 246 (2012).
51. P. Serra-Crespo, E. V. Ramos-Fernandez, J. Gascon and F. Kapteijn, *Chem. Mater.*, **23**, 2565 (2011).
52. S. Shishatskiy, J. R. Pauls, S. P. Nunes and K.-V. Peinemann, *J. Membr. Sci.*, **359**, 44 (2010).
53. W. Linfang, M. Lei, W. Aiqin, L. Qian and T. Zhang, *Chinese J. Catal.*, **28**, 805 (2007).
54. J. Duan, M. Higuchi, R. Krishna, T. Kiyonaga, Y. Tsutsumi, Y. Sato, Y. Kubota, M. Takata and S. Kitagawa, *Chem. Sci.*, **5**, 660 (2014).
55. V. Zeleňák, M. Badaničová, D. Halamova, J. Čejka, A. Zukal, N. Murafa and G. Goerigk, *Chem. Eng. J.*, **144**, 336 (2008).
56. S. Takahashi and D. Paul, *Polymer*, **47**, 7519 (2006).
57. S. Matteucci, V. A. Kusuma, D. Sanders, S. Swinnea and B. D. Freeman, *J. Membr. Sci.*, **307**, 196 (2008).
58. A. Shariati, M. Omidkhah and M. Z. Pedram, *Chem. Eng. Res. Des.*, **90**, 563 (2012).
59. H. Rabiee, A. Ghadimi and T. Mohammadi, *J. Membr. Sci.*, **476**, 286 (2015).
60. J. Adewole, A. Ahmad, S. Ismail and C. Leo, *Int. J. Greenh Gas Control*, **17**, 46 (2013).
61. L. M. Robeson, *J. Membr. Sci.*, **62**, 165 (1991).
62. L. M. Robeson, *J. Membr. Sci.*, **320**, 390 (2008).
63. A. Jomekian, R. M. Behbahani, T. Mohammadi and A. Kargari, *J. Nat. Gas Sci. Eng.*, **31**, 562 (2016).
64. Y. Dai, X. Ruan, Z. Yan, K. Yang, M. Yu, H. Li, W. Zhao and G. He, *Sep. Purif. Technol.*, **166**, 171 (2016).
65. V. Nafisi and M.-B. Hägg, *J. Membr. Sci.*, **459**, 244 (2014).
66. R. S. Murali, A. F. Ismail, M. A. Rahman and S. Sridhar, *Sep. Purif. Technol.*, **129**, 1 (2014).